Design of active Nickel single-atom decorated MoS2 as a pH-universal catalyst for hydrogen evolution reaction

Wang, Qi; Zhao, Z; Dong, S; He, Dongsheng; Lawrence, Matthew; Han, Shaobo; Cai, Chao; Xiang, Shuhuai; Rodriguez, Paramaconi; Xiang, Bin; Wang, Zhiguo; Liang, Yongye; Gu, Meng

DOI:
10.1016/j.nanoen.2018.09.003

Document Version
Peer reviewed version

Citation for published version (Harvard):
Wang, Q, Zhao, Z, Dong, S, He, D, Lawrence, M, Han, S, Cai, C, Xiang, S, Rodriguez, P, Xiang, B, Wang, Z, Liang, Y & Gu, M 2018, 'Design of active Nickel single-atom decorated MoS2 as a pH-universal catalyst for hydrogen evolution reaction', *Nano Energy*, vol. 53, pp. 458-467. https://doi.org/10.1016/j.nanoen.2018.09.003

Design of active Nickel single-atom decorated MoS_2 as a pH-universal catalyst for hydrogen evolution reaction

Qi Wang[a], Zhi Liang Zhao [a], Sha Dong[b], Dongsheng He[a], Matthew J. Lawrence[c], Shaobo Han[a,b], Chao Cai[a,b], Shuhuai Xiang[a], Paramaconi Rodriguez[c], Bin Xiang[d], Zhiguo Wang[b*], Yongye Liang[a*], Meng Gu[a*]

a. Department of Materials Science and Engineering, Southern University of Science and Technology, Shenzhen, 518055, China
b. School of Electronics Science and Engineering, University of Electronic Science and Technology of China, Chengdu, 610054, P.R. China
c. School of Chemistry, University of Birmingham, Edgbaston, Birmingham B15 2TT, UK
d. Department of Materials Science & Engineering, University of Science and Technology of China, Hefei 230026, PR China

Qi Wang, Zhi Liang Zhao and Sha Dong contributed equally to this paper

Corresponding Author: **liangyy@sustc.edu.cn; zgwang@uestc.edu.cn; gum@sustc.edu.cn ;**

Abstract: MoS_2 has been considered as a potential alternative to Pt-based catalysts in the hydrogen evolution reaction (HER). However, the presence of the inactive in-plane domains limits their surface area specific activity of the catalyst. Here, we demonstrate a new approach for activating these inactive sites and therefore dramatically enhancing the activity. We discover that decorating single Ni atom on MoS_2 can increase the HER activity in both alkaline and acidic conditions. Experimental and theoretical results indicate that single Ni atom modifiers are inclined to single dispersion in the S-edge sites and H-basal sites of MoS_2, resulting in a favorable change in the adsorption behavior of H atoms on their neighboring S atoms and subsequently the HER activity. Consequently, the single-Ni-atom decorated MoS_2 (Ni_{SA}-MoS_2) achieved cathodic current density of 10 mA cm^{-2} at overpotentials of 98mV and 110 mV in 1 M KOH and 0.5 M H_2SO_4, respectively. The dispersion of the Ni single atoms in the Ni_{SA}-MoS_2 is unaffected upon 2000 cycles in both acidic and alkaline conditions. This single atom decorating approach presents a facile and promising pathway for designing active electrocatalysts for energy conversion and storage.

Keywords: Ni Single atom, MoS_2, Hydrogen Evolution Reaction, Active sites

1. Introduction

Water splitting and hydrogen storage have the potential to boost the implementation of green energy technologies due to its high energy density and environmental-friendliness.[1,2] The electrocatalytic hydrogen evolution reaction (HER) is regarded as one of the most effective pathways to produce hydrogen.[3–5] Currently, the best known HER electrocatalysts are based on noble metals, in particular, platinum.[6] However, upon implementation in electrolyzers and fuel cells, the cost of the utilization of Pt in these technologies would limit their commercialization and industrialization due to its scarcity and high cost.[7] Therefore, the development of cost-effective HER electrocatalysts with high activities is of great significance to the hydrogen economy[8–10]

The identification of MoS_2-based materials as efficient HER electrocatalysts presented a viable class of nonprecious materials to the field.[11–13] Nevertheless, the catalytic activities of MoS_2 based materials are still inferior to the traditional Pt-based catalysts, stemming from its low active sites to surface area ratio and poor conductivity.[14] The HER catalytic sites of MoS_2 have been demonstrated to be the low coordination metallic edges whose electronic structure significantly differs from the catalytically inactive basal planes.[14] Thus, many strategies have been employed targeting the improvement in catalytic performance of MoS_2, such as controlling morphology and structure and compositing with other materials so as to expose more edge sites and accelerate electron transport speeds.[15–20] Decorating MoS_2 with foreign materials, such as Pt, Pd and metal oxide particles, has been shown to be an effective method to accelerate HER catalytic performance due to the activation of the basal plane via synergistic effect between MoS_2 and the decorating materials.[21–25] However, most of the currently reported decorating materials refer to metal particles, quite often of expensive noble metals whilst other more abundant metals suffered from instability under acidic conditions.[26,27] To date, efforts to develop low-cost MoS_2-based HER catalysts with efficient and stable performance, in both acidic and alkaline conditions have faltered.

In this work, we propose an alternative strategy to engineer MoS_2 nanosheets, resulting in significant enhancement for the HER catalysis, via decorating with single atoms of Ni in specific sites. The preparation procedure involves the synthesis of MoS_2 nanosheets supported on carbon cloth by hydrothermal method and subsequent single Ni atom decorating by wet-impregnation and calcination. Our results demonstrate that single atom Ni-decorated MoS_2 (Ni_{SA}-MoS_2/CC) catalysts exhibit superior electrocatalytic activities toward HER in both acidic and alkaline media, which is attributed to the activation of the sites at S-edge and the originally inert basal plane of MoS_2 by coordination of single Ni atoms. We also demonstrate the good stability of the Ni single atom decorated on the MoS_2 nanosheet through potential cycling.

2. Material and methods

2.1 Materials preparation

1. Synthesis of MoS_2nanosheets array on carbon clothes (MoS_2/CC)

0.25 g Na_2MoO_4 and 0.3 g thiourea was added into 18 ml H_2O, after stirring for 10 min, the solution was transferred into 50 ml Teflon-lined stainless autoclave. After a piece of carbon cloth was immersed in the solution for 10 min, placed in the stainless autoclave was sealed and heated at 220 ℃ for 24 h. the pr rinsed with deionized (DI) water and ethanol three times.

2. Synthesis of Ni_{SA}- MoS_2/CC

A piece of MoS_2/CC was immersed into $NiCl_2$ ethanol solution (4 mg/mL) for 10s, then taken out and dried at 80 ℃ and the product was annealed at 300 ℃ for 1h under the 10 % H 2 atmosphere. Then sample was purified with DI water and ethanol.

3. Synthesis of Ni_C-MoS_2/CC

A piece of MoS_2/CC was immersed into $NiCl_2$ ethanol solution(4mg/mL) for 10s, then taken out and dried at 80 ℃ and the product was annealed at 600 ℃ for 2 h under the 10% H 2 atmosphere. Then sample was purified with DI water and ethanol.

2.2 Characterization

The phase of the as-prepared products was identified by XRD with Cu Kα radiation (λ = 1.5418 Å). Scanning electron microscope (SEM) images were taken on a FEI Helios Nanolab 600i scanning electron microscope. Room-temperature HAADF-STEM imaging and Electron Energy Loss Spectroscopy (EELS) were conducted using a double Cs-corrected Themis Z S/TEM operated at an accelerating voltage of 60-300 kV. The XPS analyses were carried out on a PHI 5000 VersaProbe II spectrometer using monochromatic Al K(alpha) X-ray source.

2.3 Electrochemical testing

Electrochemical measurements of the as-prepared samples towards the hydrogen evolution reaction (HER) were conducted at room temperature in a standard three-electrode cell, with a 0.5 M H_2SO_4 solution and 1M KOH solution were used as the electrolyte. A piece of freshly-made MoS_2/CC, Ni_{SA}- MoS_2/CC or Ni_C-MoS_2/CC as the working electrode, a graphite rod as the counter electrode and a saturated calomel electrode (SCE) as the reference electrode. In all measurements, the SCE was calibrated with respect to RHE. In 0.5 M H_2SO_4, E (RHE) = E (SCE) + 0.241 V. In 1.0 M KOH, E (RHE) = E (SCE) + 1.068 V. LSV curves were conducted in electrolyte with a scan rate of 5 $mV \cdot s^{-1}$. All the potentials reported in our work were expressed vs. the RHE.

2.4 Simulation details and methods

All the calculations were performed by using density functional theory (DFT) calculations as implemented in the Vienna *ab initio* package (VASP). Spin-polarization was considered for all the simulations. The projector augmented wave (PAW) method was used to describe electron-ion interaction, while the generalized gradient approximation using the Perdew-Burke-Ernzerhof (PBE) functional was used to describe the electron exchange-correlation.[28] A plane wave basis was set up to an energy cutoff of 520 eV. A 30 Å vacuum space was constructed to avoid the periodical image interactions between two adjacent MoS_2 layers. The Brillouin zone was integrated using the Monkhorst-Pack scheme with 3×3×1 *k*-grid.[29] All the atomic positions and cell parameters were relaxed using a conjugate gradient minimization until the force on each atom is less than 0.01 eV/Å.

The adsorption energy (E_{ads}) of Ni on monolayer $MoS_2$and slab were calculated with $E_{\mathrm{ads}} = E_{\mathrm{MoS_2+Ni}} - E_{\mathrm{MoS_2}} - E_{\mathrm{Ni}}$,[30] where $E_{\mathrm{MoS_2+Ni}}$ and $E_{\mathrm{MoS_2}}$ are the total energies of MoS_2 with and without Ni adsorption, respectively. E_{Ni} is the energy of an isolated Ni atom.

The formation energy (E_{f}) for the substitution of Mo with Ni was calculated with $E_{\mathrm{f}} = E_{\mathrm{Ni-Mo}} - E_{\mathrm{MoS_2}} + \mu_{\mathrm{Mo}} - \mu_{\mathrm{Ni}}$,where $E_{\mathrm{Ni-Mo}}$ and $E_{\mathrm{MoS_2}}$are the total energies of MoS_2 with and without Ni substitution, respectively. $\mu_{\mathrm{Mo}}$and μ_{Ni} were the chemical potentials of Mo and Ni atoms, respectively. μ_{Mo} and μ_{Ni}values were calculated with respect to the bulk state.

Gibbs free-energy of the adsorption atomic hydrogen was calculated using equation (1):

$$\Delta G_{\mathrm{H}} = \Delta E_{\mathrm{H}} + \Delta E_{\mathrm{ZPE}} - T\Delta S_{\mathrm{H}} \quad (1)$$

where ΔE_{ZPE} and ΔS_{H} are the zero-point energy and entropy difference of hydrogen in the adsorbed state and the gas phase, respectively. The hydrogen adsorption energy ΔE_{H} is calculated with the following expression:

$$\Delta E_{\mathrm{H}} = E_{\mathrm{MoS_2-H}} - E_{\mathrm{MoS_2}} - \frac{1}{2}E_{\mathrm{H_2}} \quad (2)$$

where $E_{\mathrm{MoS_2-H}}$ and $E_{\mathrm{MoS_2}}$ are the total energies of MoS_2 with and without hydrogen adsorption, respectively. $E_{\mathrm{H_2}}$ is the energy of a gas phase hydrogen molecule.

The calculated frequencies of H_2 gas were 4345 cm^{-1}, 58 cm^{-1}, and 42 cm^{-1}. The contribution from the configurational entropy in the adsorbed state is small and is neglected. So the entropy of hydrogen adsorption as $\Delta S_{\mathrm{H}} = \frac{1}{2}E_{\mathrm{H_2}}$ where S_{H_2} is the entropy of molecule hydrogen in the gas phase at standard conditions[31]. With these values the Gibbs free energy of equation (1) can be rewritten as:

$$\Delta G_{\mathrm{H}} = \Delta E_{\mathrm{H}} + 0.29 \quad (3)$$

2. Results and Discussion

The self-supported MoS_2-carbon cloth (MoS_2/CC) electrodes were synthesized by growing MoS_2 on a pre-treated carbon cloth through a hydrothermal method.[32] The single atom modification was achieved by wet-impregnation of the MoS_2/CC in $NiCl_2$ solution and further calcination in a 10% H_2/Ar atmosphere at 300 ℃ for 1h. The synthetic procedure employed in the production of Ni_{SA}-MoS_2/CC is illustrated in Figure 1. In order to demonstrate the effect of the single atom decorating on the MoS_2, a Ni-cluster modified MoS_2 (Ni_C-MoS_2/CC) was prepared by minor modification of the synthetic method. In this case, the wet-impregnated

MoS_2/CC sample was calcined at 600℃ for 2h under 10% H_2/Ar atmosphere. Full experimental details can be found in the experimental procedure section.

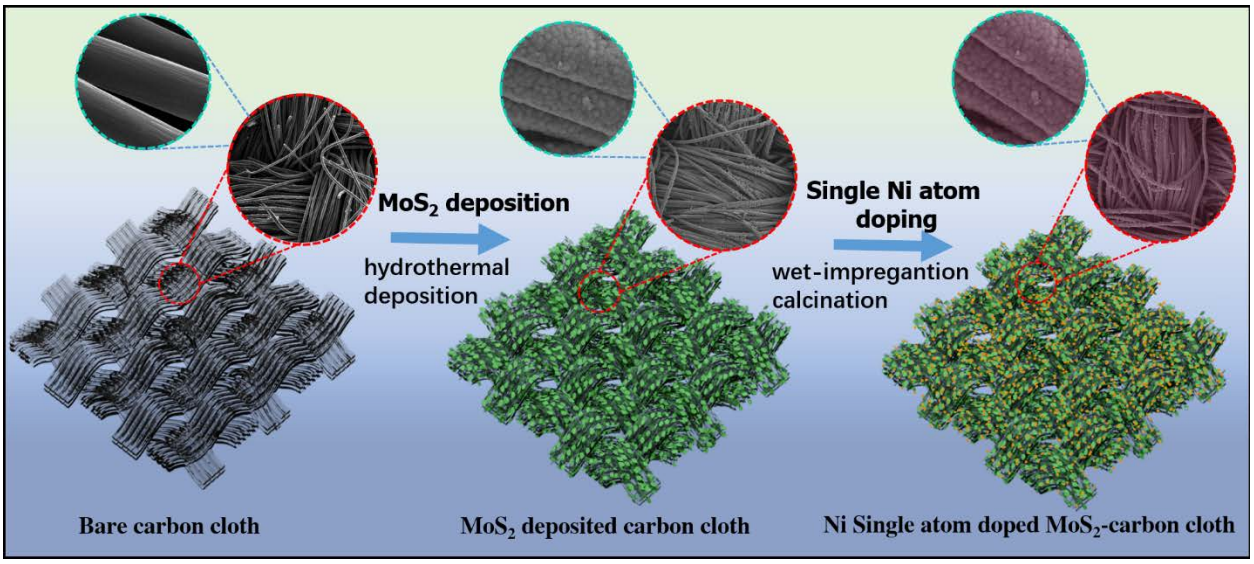

Figure 1 Schematic procedure for the preparation of Ni_{SA}-MoS_2 and Ni_C-MoS_2.The green color of the cartoon represent the MoS_2 deposited catalyst, the orange dots correspond to the Ni-single atom decorating of the MoS_2. Top figure in circles correspond to the SEM images of the sample at each stage of the preparation.

SEM images of the original MoS_2 indicate that the carbon cloth substrate is fully covered with the MoS_2 nanosheet array (Figure S1). The low- and high-magnification SEM images of Ni_{SA}-MoS_2 presented in Figure 2a-b suggest that both the morphology and integrated nature of the nanosheet array are well preserved upon Ni decorating. The high uniformity and coverage of the as-prepared sample is evidenced by SEM images captured at various magnifications (Figure S2). Figure 2d shows the X-ray diffraction (XRD) patterns of MoS_2/CC and Ni_{SA}-MoS_2/CC. For the MoS_2/CC precursor, the diffraction peaks at ~2θ= 32.8°, 39.7° and 58.3° correspond well to the (100), (103) and (110) planes of the hexagonal MoS_2 phase (JCPDS no. 37-1492), respectively. The composition of Ni was also determined by ICP-AES to be 1.8±0.1 at.%. No obvious change in the relative signal intensity or position of the MoS_2 peaks is observed after Ni atom decorating. No additional peaks are observed, which can be attributed to the low concentration of highly dispersed Ni atoms.

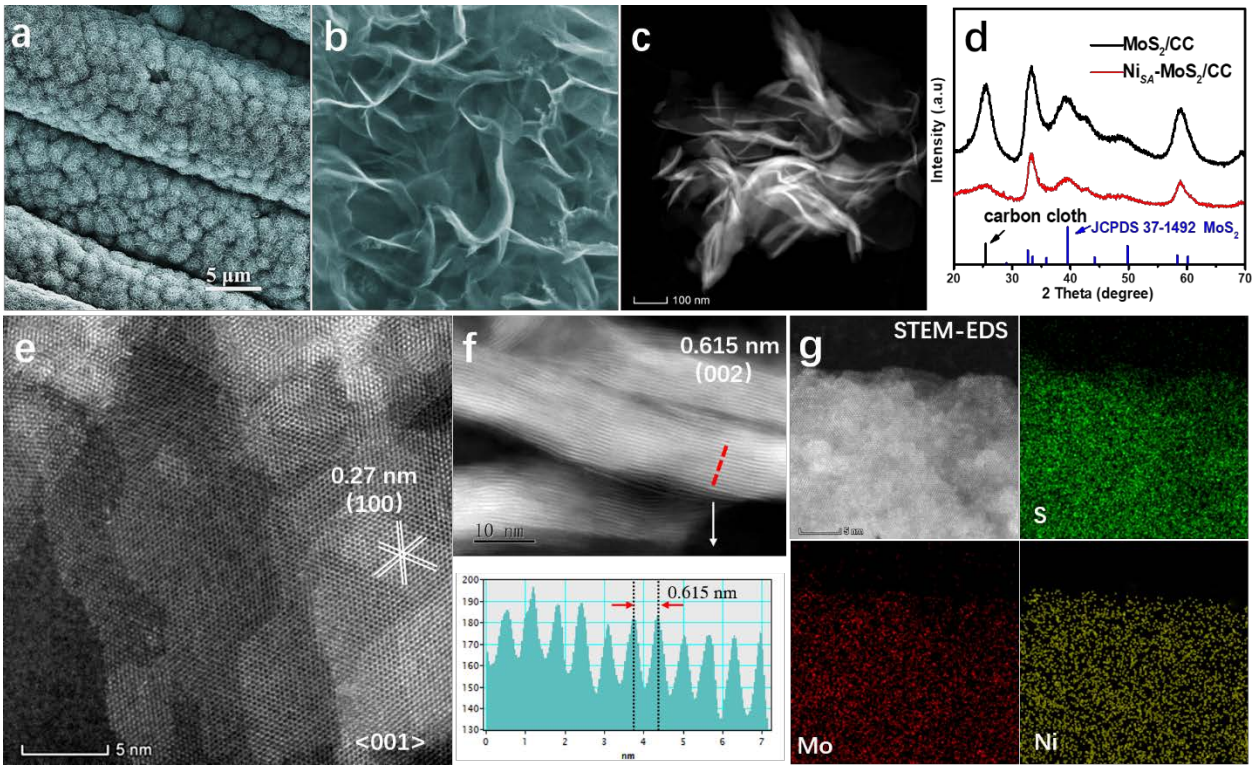

Figure 2 (a) Low and (b) high magnification SEM images of Ni_{SA}-MoS_2/CC, (c) HAADF-STEM image in low magnification (d) XRD spectrum of Ni_{SA}-MoS_2/CC and undecorated MoS_2/CC. Atomic STEM images of (e) basal plane and (f) edge site of Ni_{SA}-MoS_2/CC.(g) EDS-mapping of Ni_{SA}-MoS_2/CC.

Fig. 2c shows a typical STEM image of the MoS_2 nanosheet. The spacing of the crystal lattices, as shown in Figure 2e, is 0.27 nm, which can be attributed to basal planes of MoS_2 viewed along the <001> zone axis.

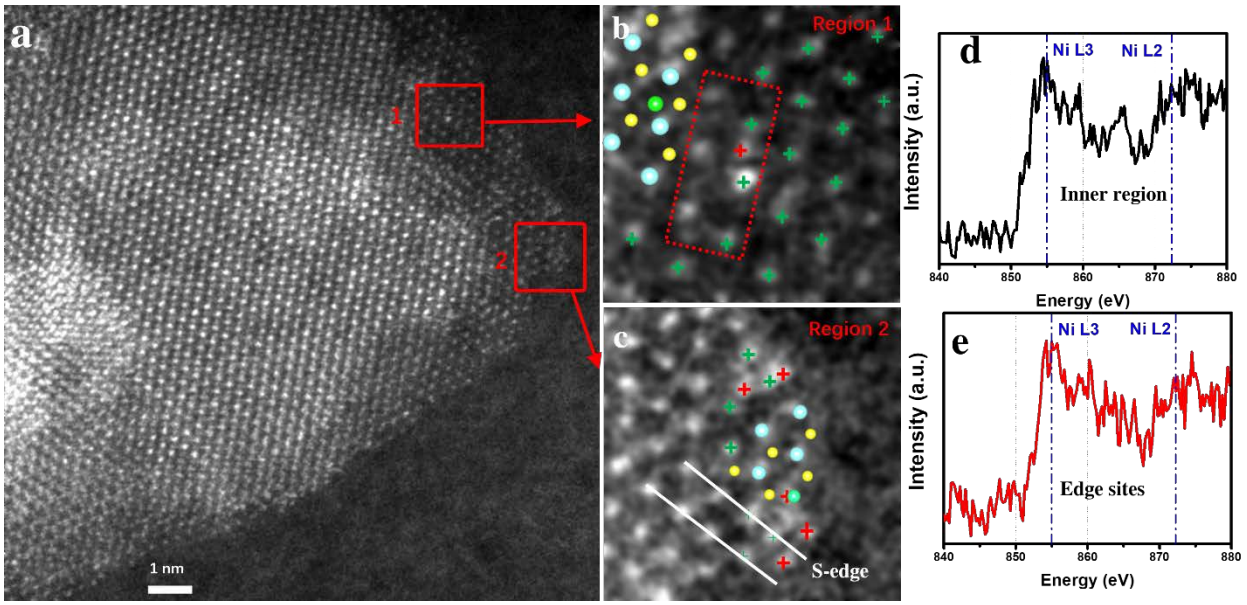

Figure 2f shows the fringes of the layered nanosheet arrays. The profile indicates the layer distance to be 0.615 nm, which is in accordance with the layer distance of MoS_2.[33] The high density of edge sites observed in these regions indicates the edge-rich feature of Ni_{SA}-MoS_2/CC, which is favorable to HER activity.[14] Besides, no Ni cluster or particles were observed at any region of the Ni_{SA}-MoS_2/CC samples, indicating the highly dispersed nature of the Ni atoms. Distribution of Ni atoms in the MoS_2 nanosheet is further corroborated by scanning transmission electron microscopy coupled energy-dispersive X-ray spectroscopy (STEM-EDS) element mapping (Figure 2g). It is evident that Ni atoms are uniformly dispersed and that no areas of aggregation are detected. The Ni content in the product was calculated to be 1.9±0.1 at.% from the mapping, which is in good agreement with the ICP-AES result. In contrast, the Ni_c-MoS_2/CC shows Ni cluster size ranged between 4-13 nm and the atomic ratio of Ni in this sample was slightly larger (2.0±0.1 at.%) (see Supplementary Figure3).

Figure 3 (a) Atomic resolution STEM images of NiSA-MoS_2/CC and corresponding close-up views of (b) region 1 and (c) region 2; Ni atoms marked with a red cross, Mo atoms marked with a green cross) Corresponding Ni EELS spectra of (d) inner region 1 and (e) edge sites, region 2

The coordination of the Ni decorating site can impose a significant effect on the HER performance of MoS_2-based catalysts.[23] Some previous reported works have illuminated a Ni doping strategy to modify MoS_2 lattice in order to improve its HER performance.[11,23,34] In their cases, Ni atoms substitute some Mo sites in MoS_2 lattice. However, the 300 °C calcination of $NiCl_2$ upon a well-formed MoS_2 in this work may result in a totally different Ni atoms location. To verify the coordination of Ni atoms in the MoS_2 lattice in this work, atomic resolution STEM was applied. The HAADF-STEM image, shown in Figure 3a, presents a high magnification view of a piece of Ni_{SA}-MoS_2/CC. No obvious Ni atom could be found due to the lower atomic number of Ni in comparison to Mo. By analyzing the atomic structure of larger multiples, some embedded foreign atoms are found in the atomic column of MoS_2 (Figure 3b, c). The corresponding EELS spectra of this sites reveal the existence of Ni peaks at ~855 eV, suggesting the embedded atoms to be Ni atoms (Figure 3d). Figure 3b shows a magnified image of the Ni atom from Figure 3a (region 1), demonstrating the single Ni atom locates atop of a hexagonal site of the basal plane, namely H-basal site. The model inserted is an atomic simulation of the red rectangle region. Moreover, the high density of disordered atoms with lower contrast, situated at the edge of MoS_2, suggests the existence of Ni atoms in the S-edge (Figure 3c). The corresponding EELS spectra of edge sites also reveal these atoms to be Ni atoms (Figure 3e).[35] The signals obtained in both regions were rough due to the atomic dispersion of Ni atoms.[36]

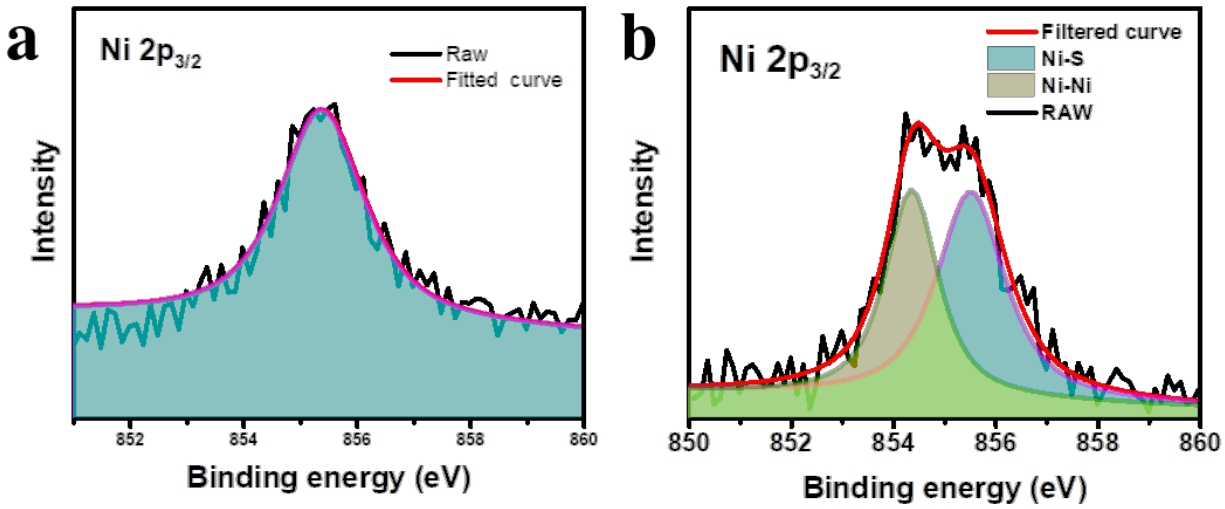

Figure 4 Ni $2p_{3/2}$ XPS spectrum of (a) Ni_{SA}-MoS_2/CC and (b) Ni_c-MoS_2/CC.

The chemical coordination of Ni atoms can largely influence their activity and stability during catalysis. The Ni surface composition and electronic binding energies were characterized by X-ray photoelectron

spectroscopy (XPS) with C 1s energy correction (see Figure S4). The Ni $2p_{3/2}$ spectrum of Ni_{SA}-MoS_2/CC shows a single peak located at 855.5 eV, which can be assigned to Ni-S bonding (Figure 4a).[37] In comparison, the Ni $2p_{3/2}$ spectrum of Ni_c-MoS_2/CC shows two characteristic peaks located at 854.5 eV and 855.5 eV, which can be assigned as Ni-Ni and Ni-S bonding, respectively (Figure 4b).[37] These results provide further evidence for the single atom dispersion of Ni in Ni_{SA}-MoS_2/CC. The noticeable signal noise is attributed to the high dispersion and low concentration of Ni atoms. [38]

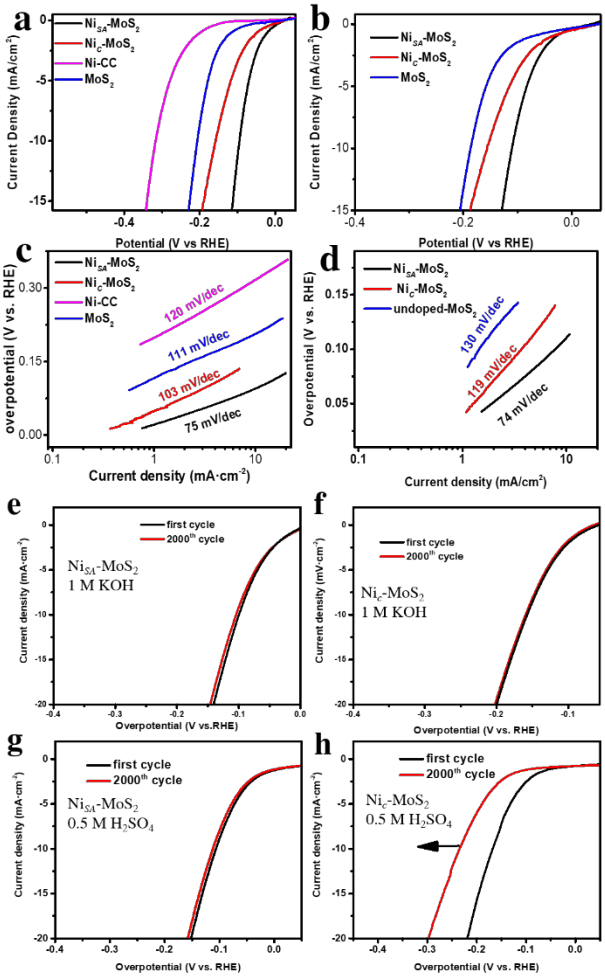

Figure 5 (a) Polarization curves of Ni_{SA}-MoS_2/CC, Ni_c-MoS_2/CC, Ni/CC and MoS_2/CC in 1 M KOH solution with a scan rate of 5 mV·s^{-1}. (b) Polarization curves of Ni_{SA}-MoS_2, Ni_c-MoS_2 and bare MoS_2 in 0.5 M H_2SO_4 solution with a scan rate of 5 mV·s^{-1}. (c) Tafel plots obtained from the polarization curves in (a). (d) Tafel plots obtained from the polarization curves in (b). Stability tests by measuring the polarization profiles for Ni_{SA}-MoS_2/CC (e,g) catalyst and Ni_c-MoS_2/CC before and after 2000 cyclic potential scans in 1 M KOH (e,f) and 0.5 M H2SO4 (g,h) at a scan rate of 50 mV·s^{-1}.

Inspired by the unique structural features of Ni_{SA}-MoS_2/CC, its HER activity was firstly evaluated in 1 M KOH solution. For comparison, the HER performance of Ni/CC, MoS_2/CC and Ni_c-MoS_2/CC were also investigated under identical conditions. Since the as-measured reaction currents cannot directly reflect the intrinsic behavior of the catalysts due to the effect of Ohmic resistance, an iR compensation was applied to all recorded data. Figure 5a shows representative linear sweep voltammograms (LSVs) of the aforementioned catalysts in 1 M KOH. For Ni_{SA}-MoS_2/CC, an overpotential of ~95 mV versus reversible hydrogen electrode (RHE) is needed to drive a cathodic current density of 10 $mA \cdot cm^{-2}$, which is 112 mV lower than that of MoS_2/CC (207 mV) and 62 mV lower than that of Ni_c-MoS_2/CC (157 mV). Such activity surpasses most of previously reported metal sulfide HER electrocatalysts.[39–41] It is noted that the HER activity of MoS_2 is significantly enhanced after Ni decorating in the form of either clusters or single atoms, which can be attributed to the synergistic effect of Ni at the catalyst surface, the HER mechanism can be generalized for two pathways: (Scheme 1) the Volmer-Heyrovsky mechanism and/or (Scheme 2) the Volmer-Tafel mechanism (See Supplementary Scheme). These two pathways imply that the competitive processes of H-atom adsorption/desorption occurring at the catalyst surface should be matched in order to accelerate the HER. Hydrogen adsorption (H_{ads}) in alkaline condition is formed from dissociation of water. This step is rather sluggish on MoS_2 surface, which is the main inhibitor of the reaction.[42] However, water dissociation is accelerated at Ni atom sites, resulting in the enhanced HER activity observed for Ni_{SA}-MoS_2/CC.[43] A HER catalyzed by pure MoS_2 follows the Volmer-Heyrovsky mechanism (scheme 1),[22] which has a lower H_{ads} coverage (Θ_H) and a Tafel slope of ~111 $mV \cdot decade^{-1}$. In contrast, the Ni_{SA}-MoS_2/CC shows a Tafel slope of 75 $mV \cdot decade^{-1}$, which is about 36 $mV \cdot decade^{-1}$ lower than that of MoS_2/CC and 45 $mV \cdot decade^{-1}$ less than that of Ni-decorated carbon cloth (Ni/CC) (Figure 5c). The Tafel slope of 75 $mV \cdot decade^{-1}$ indicates that the rate-limiting step at low overpotentials is the recombination of two adsorbed H atoms, which demonstrates that that the Ni decorating promotes the HER via a Volmer-Tafel mechanism (Scheme 2). When comparing the Ni_{SA}-MoS_2/CC with the Ni_c-MoS_2/CC, it was observed that the presence of Ni cluster favors the HER (Tafel slope of 103 $mV \cdot decade^{-1}$) relative to MoS_2/CC. However, the catalytic activity of the Ni_{SA}-MoS_2/CC is significantly superior with respect to the Ni_c-MoS_2/CC. This result demonstrates that single atom Ni-decorating in MoS_2 is preferable to cluster-decorating in the pursuit of a more efficient HER catalyst. Furthermore, the LSVs of Ni_{SA}-

MoS_2/CC and Ni_c-MoS_2 suffers negligible depletion before and after 2000 cycles, suggesting the Ni single atoms can stablely anchor on MoS_2 in alkaline condition (Figure 5e,f).

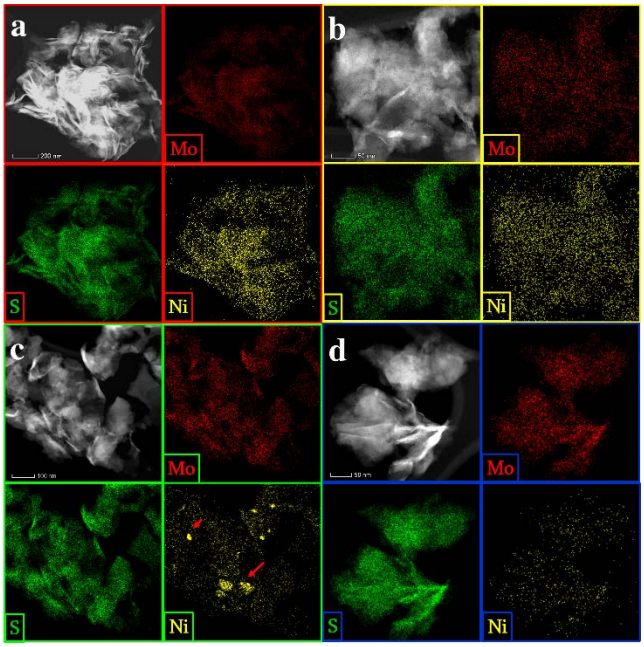

Figure 6 EDS-mapping of Ni_{SA}-MoS_2/CC sample before (a) and after (b) 2000 CV cycle in 0.5M H_2SO_4 solution. The Ni amount suffers no obvious change after 2000 cycles. EDS-mapping of Ni_c-MoS_2/CC sample before (c) and after (d) 2000 CV cycle in 0.5M H_2SO_4 solution. A huge depletion of Ni (2.0 at.% to 0.7 at.%, evidenced by ICP-AES) was found after 2000 cycles caused by the dissolution of Ni atom in the harsh electrochemical condition.

The HER performance of as prepared sample was further studied in a 0.5 M H_2SO_4 solution. It took an overpotential of 110 mV to achieve a current density of 10 $mA \cdot cm^{-2}$, 47 mV lower than that of Ni_c-MoS_2/CC (157mV) and 76 mV lower than that of the undecorated MoS_2/CC (186 mV). Meanwhile, Ni_{SA}-MoS_2/CC showed a Tafel slope of 74 $mV \cdot decade^{-1}$ which is lower than Ni_c-MoS_2/CC (119 $mV \cdot decade^{-1}$) and undecorated MoS_2 (130 $mV \cdot decade^{-1}$), indicating a superior HER catalytic activity of single atom decorating in acid environment. Additionally, the stability of Ni_{SA}-MoS_2/CC was examined by successive 2000 CV cycles in

a 0.5 M H_2SO_4 solution (Figure 5g). Little decrease was observed after 2000 CV cycles. However, overpotential of Ni_c-MoS_2/CC suffered great depletion in the same condition. EDS results revealed that Ni atoms in Ni_{SA}-MoS_2/CC still dispersed homogeneously and the loading amount suffered little decrease (Figure 6a,b). In contrast, Ni cluster in Ni_c-MoS_2/CC vanished after CV cycles (Figure 6c,d) and the overpotential increased from ~167 mV to ~234 mV due to Ni cluster losing after 2000 cycles (Figure 5h). We attribute the stability of Ni single atom to the strengthened Ni-S bonding.[44]

Density functional theory (DFT) calculations were performed to gain fundamental understanding of the

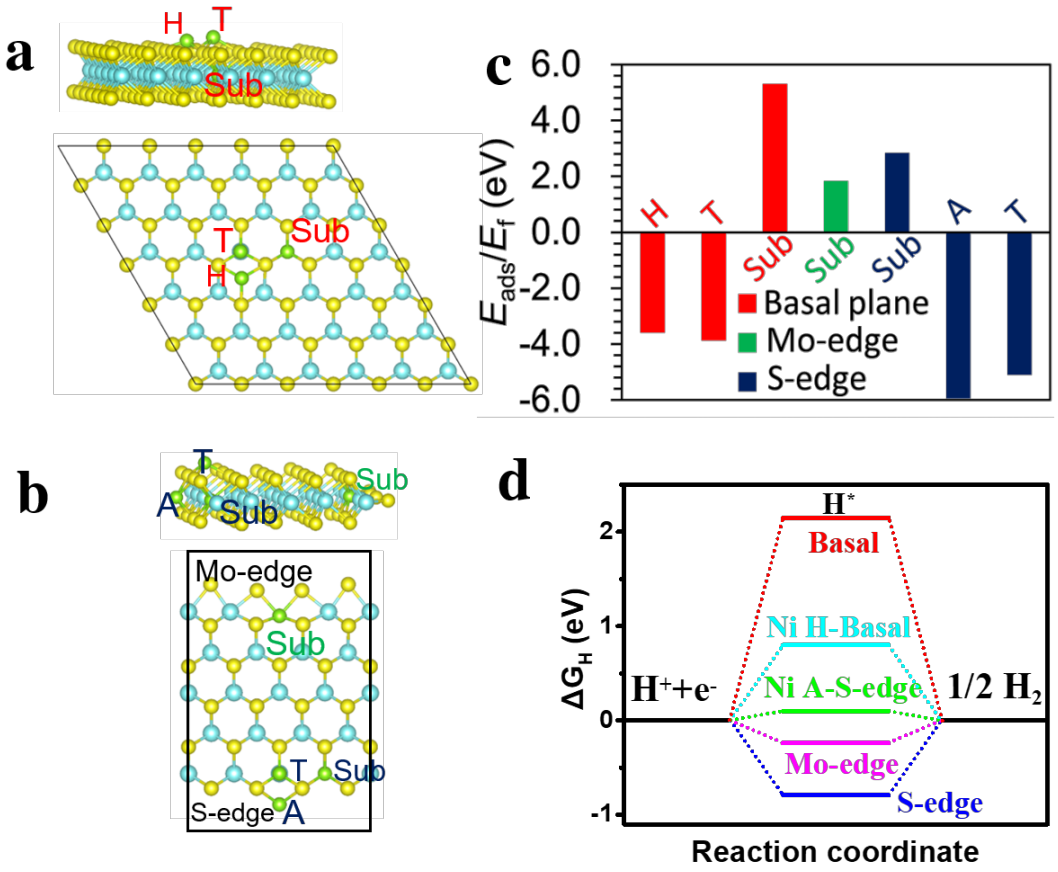

Figure 7 (a) Atomistic configuration of Ni absorbed at the top of the Mo sites (T) and the center of the hexagon sites (H) on the basal plane and substitution of Mo atom with Ni in monolayer MoS_2. (b) Atomistic configuration of Ni absorbed at T and A sites at the S-edge and substitution of Mo atom with Ni at the Mo-edge and S-edge. (c) Adsorption energy of Ni on MoS_2 and formation energy of substitution of Mo atom with Ni atom in MoS_2. (d) Gibbs free energies for H* adsorbed at basal plane, Mo edge and S edge with and without Ni adsorption/substitution.

Ni_{SA}-MoS_2 active sites during the HER under alkaline conditions. First, the possible atomistic configurations of Ni-MoS_2 were evaluated. Two possible adsorption sites for Ni on the basal plane of MoS_2 are the top of the Mo site (T) and the center of the hexagonal sites (H) (Figure 7a). The Ni can also be coordinated at the S-edge in MoS_2, as shown in Figure 7b. Thus, there were three substitution sites for Ni replacing Mo, i.e. the basal plane, the Mo-edge and the S-edge of MoS_2. It was reported that the Mo-edge covered with S atoms is catalytically active for the HER,[45] and we adopted the same model. Details of the simulation methodology can be found in the Supporting Information.

Figure 7c shows the calculated E_{ads} and E_{f} values; positive values indicate unfavorable interactions. The adsorption of Ni is preferential at the A site of the S-edge, in addition to the T-site and H-site of the basal plane. The E_{f} values are 5.30, 1.83 and 2.83 eV for the substitution of Ni for Mo at the basal plane, the Mo-edge and the S-edge, respectively, indicating the less possibility of that the substitution of Mo with Ni. As was discussed above, the presence of Ni atoms at the A-S-edge and H-basal site was confirmed by atomic STEM, indicating good agreement between the experimental observation and the theoretical results.

The Gibbs free-energy for the adsorption of atomic hydrogen (ΔG_{H}) , which should be close to zero for an ideal HER catalyst, is an important parameter to discuss in the evaluation of the HER catalyst. Thus, we calculated ΔG_{H} at the basal plane, Mo-edge and S-edge in the absence and presence of Ni-decorating. The free energy diagrams for HER are shown in Figure 7d. The +2.16 eV value for the basal plane of MoS_2 indicates that H^+ cannot be efficiently adsorbed there. A ΔG_{H} = -0.79 eV at the S-edge indicates that H_2 cannot effectively desorb from the S-edge. On the other hand, a $\Delta G_{\mathrm{H}} \cong$ -0.24 at the Mo-edge, is distinctive as a good HER active site. Our results are in good agreement with previous reports that the catalytically active sites of monolayer MoS_2 are located at the Mo-edge, while the basal plane is inert to the HER.[46] Interestingly, after single Ni atoms are anchored on S-edge, the value of ΔG_{H} are calculated to be 0.1 eV, indicating the introduction of a great enhanced HER active sites. Additionally, the calculations on the Ni_{SA}-MoS_2 show that the values of ΔG_{H} for the H-basal sites decrease to 0.8 eV, suggesting an improvement in the HER activity of the basal plane. Thus, single Ni atom-decorating does not significantly affect the catalytic behavior of the Mo-edge, but rather promotes noticeable improvement in the catalytic activity of S-edges. The inert basal plane is activated and the activity of the edge sites is greatly enhanced. In this case, Ni_c-MoS_2, with the same

decorating concentration, provides less activated sites in comparison to Ni_{SA}-MoS_2. The Ni_{SA}-MoS_2 can offer a synergistic effect along with activated effect so as to provide higher HER activity.[22]

3. Conclusions

In conclusion, through introducing Ni single atoms into the MoS_2 S-edge and H-sites of the basal plane, a distinct enhancement of HER activity was achieved compared with pure MoS_2/CC and Ni cluster-decorated MoS_2/CC. Atomic STEM indicates that the Ni single atoms were anchored on the S-edge and H sites of basal plane. Experimentally, by decorating the MoS_2 with Ni-single atoms, the overpotential to achieve a current density of 10 $mA \cdot cm^{-2}$ during the HER is significantly reduced in comparison to undecorated MoS_2 and Ni-cluster decorated MoS_2 in acidic conditions. DFT calculations indicate that the decorated Ni atoms on the S-edge and H site of basal plane can tune the adsorption behavior of H atoms and consequently the HER activity. The Ni_{SA}-MoS_2/CC provides a low-cost but highly efficient solution to HER. This work opens the door to the design of more active catalyst based on single-atom decorating MoS_2 with other transition metal, which can outperform the catalytic activity of state of the art catalyst without the utilization of precious metals.

Acknowledgments

M.G. and Y. L. want to acknowledge the support from 1000 Talents Plan of China. The TEM work was performed at the SUSTech Pico center that receives funding from the Shenzhen government. Z.W. was financially supported by the National Natural Science Foundation of China (11474047). Dongsheng He was financially supported by the National Natural Science Foundation of China (51602143). This work was carried out at National Supercomputer Center in Tianjin, and the calculations were performed on TianHe-1(A).

References

[1] M.S. Dresselhaus, I.L. Thomas, Alternative energy technologies, Nature. 414 (2001) 332–337. doi:10.1038/35104599.

[2] J.A. Turner, Sustainable Hydrogen Production, Science (80-.). 305 (2004) 972–974. doi:10.1126/science.1103197.

[3] T. Liu, D. Liu, F. Qu, D. Wang, L. Zhang, R. Ge, S. Hao, Y. Ma, G. Du, A.M. Asiri, L. Chen, X. Sun, Enhanced Electrocatalysis for Energy-Efficient Hydrogen Production over CoP Catalyst with Nonelectroactive Zn as a Promoter, Adv. Energy Mater. 7 (2017) 1700020. doi:10.1002/aenm.201700020.

[4] H. Ou, L. Lin, Y. Zheng, P. Yang, Y. Fang, X. Wang, Tri- s -triazine-Based Crystalline Carbon Nitride Nanosheets for an Improved Hydrogen Evolution, Adv. Mater. 29 (2017) 1700008. doi:10.1002/adma.201700008.

[5] Y. Sun, K. Xu, Z. Wei, H. Li, T. Zhang, X. Li, W. Cai, J. Ma, H.J. Fan, Y. Li, Strong Electronic Interaction in Dual-Cation-Incorporated $NiSe_2$ Nanosheets with Lattice Distortion for Highly Efficient Overall Water Splitting, Adv. Mater. 30 (2018) 1802121. doi:10.1002/adma.201802121.

[6] Y. Xu, B. Zhang, Recent advances in porous Pt-based nanostructures: synthesis and electrochemical applications., Chem. Soc. Rev. 43 (2014) 2439–50. doi:10.1039/c3cs60351b.

[7] E. Kemppainen, A. Bodin, B. Sebok, T. Pedersen, B. Seger, B. Mei, D. Bae, P.C.K. Vesborg, J. Halme, O. Hansen, P.D. Lund, I. Chorkendorff, Scalability and feasibility of photoelectrochemical H_2 evolution: the ultimate limit of Pt nanoparticle as an HER catalyst, Energy Environ. Sci. 8 (2015) 2991–2999. doi:10.1039/C5EE02188J.

[8] J. Wang, F. Xu, H. Jin, Y. Chen, Y. Wang, Non-Noble Metal-based Carbon Composites in Hydrogen Evolution Reaction: Fundamentals to Applications, Adv. Mater. 29 (2017) 1605838. doi:10.1002/adma.201605838.

[9] H.-J. Qiu, Y. Ito, W. Cong, Y. Tan, P. Liu, A. Hirata, T. Fujita, Z. Tang, M. Chen, Nanoporous Graphene with Single-Atom Nickel Dopants: An Efficient and Stable Catalyst for Electrochemical Hydrogen Production, Angew. Chemie Int. Ed. 54 (2015) 14031–14035. doi:10.1002/anie.201507381.

[10] Y. Sun, L. Hang, Q. Shen, T. Zhang, H. Li, X. Zhang, X. Lyu, Y. Li, Mo doped Ni_2 P nanowire arrays: an efficient electrocatalyst for the hydrogen evolution reaction with enhanced activity at all pH values, Nanoscale. 9 (2017) 16674–16679. doi:10.1039/C7NR03515B.

[11] Q. Lu, Y. Yu, Q. Ma, B. Chen, H. Zhang, 2D Transition-Metal-Dichalcogenide-Nanosheet-Based Composites for Photocatalytic and Electrocatalytic Hydrogen Evolution Reactions, Adv. Mater. 28 (2016) 1917–1933. doi:10.1002/adma.201503270.

[12] Y. Zhu, L. Peng, Z. Fang, C. Yan, X. Zhang, G. Yu, Structural Engineering of 2D Nanomaterials for Energy Storage and Catalysis, Adv. Mater. 30 (2018) 1706347. doi:10.1002/adma.201706347.

[13] S. Jayabal, G. Saranya, J. Wu, Y. Liu, D. Geng, X. Meng, Understanding the high-electrocatalytic performance of two-dimensional MoS_2 nanosheets and their composite materials, J. Mater. Chem. A. 5 (2017) 24540–24563. doi:10.1039/C7TA08327K.

[14] T.F. Jaramillo, K.P. Jorgensen, J. Bonde, J.H. Nielsen, S. Horch, I. Chorkendorff, Identification of Active Edge Sites for Electrochemical H_2 Evolution from MoS_2 Nanocatalysts, Science (80-.). 317 (2007) 100–102. doi:10.1126/science.1141483.

[15] H. Li, C. Tsai, A.L. Koh, L. Cai, A.W. Contryman, A.H. Fragapane, J. Zhao, H.S. Han, H.C. Manoharan, F. Abild-Pedersen, J.K. Nørskov, X. Zheng, Activating and optimizing MoS_2 basal planes for hydrogen evolution through the formation of strained sulphur vacancies, Nat. Mater. 15 (2016) 48–53. doi:10.1038/nmat4465.

[16] G. Ye, Y. Gong, J. Lin, B. Li, Y. He, S.T. Pantelides, W. Zhou, R. Vajtai, P.M. Ajayan, Defects Engineered Monolayer MoS_2 for Improved Hydrogen Evolution Reaction, Nano Lett. 16 (2016) 1097–1103. doi:10.1021/acs.nanolett.5b04331.

[17] K. Chang, Z. Mei, T. Wang, Q. Kang, S. Ouyang, J. Ye, MoS_2 /Graphene Cocatalyst for Efficient Photocatalytic H_2 Evolution under Visible Light Irradiation, ACS Nano. 8 (2014) 7078–7087. doi:10.1021/nn5019945.

[18] J. Ding, Y. Zhou, Y. Li, S. Guo, X. Huang, MoS 2 Nanosheet Assembling Superstructure with a Three-Dimensional Ion Accessible Site: A New Class of Bifunctional Materials for Batteries and Electrocatalysis, Chem. Mater. 28 (2016) 2074–2080. doi:10.1021/acs.chemmater.5b04815.

[19] J. Kibsgaard, Z. Chen, B.N. Reinecke, T.F. Jaramillo, Engineering the surface structure of MoS_2 to preferentially expose active edge sites for electrocatalysis, Nat. Mater. 11 (2012) 963–969. doi:10.1038/nmat3439.

[20] J. Xie, H. Zhang, S. Li, R. Wang, X. Sun, M. Zhou, J. Zhou, X.W.D. Lou, Y. Xie, Defect-Rich MoS_2 Ultrathin Nanosheets with Additional Active Edge Sites for Enhanced Electrocatalytic Hydrogen Evolution, Adv. Mater. 25 (2013) 5807–5813. doi:10.1002/adma.201302685.

[21] X. Huang, Z. Zeng, S. Bao, M. Wang, X. Qi, Z. Fan, H. Zhang, Solution-phase epitaxial growth of noble metal nanostructures on dispersible single-layer molybdenum disulfide nanosheets, Nat. Commun. 4 (2013) 1444. doi:10.1038/ncomms2472.

[22] X. Zhang, Y. Liang, Nickel Hydr(oxy)oxide Nanoparticles on Metallic MoS_2 Nanosheets: A Synergistic Electrocatalyst for Hydrogen Evolution Reaction, Adv. Sci. 5 (2018) 1700644. doi:10.1002/advs.201700644.

[23] Y. Shi, Y. Zhou, D.-R. Yang, W.-X. Xu, C. Wang, F.-B. Wang, J.-J. Xu, X.-H. Xia, H.-Y. Chen, Energy Level Engineering of MoS_2 by Transition-Metal Doping for Accelerating Hydrogen Evolution Reaction, J. Am. Chem. Soc. 139 (2017) 15479–15485. doi:10.1021/jacs.7b08881.

[24] M. Miao, J. Pan, T. He, Y. Yan, B.Y. Xia, X. Wang, Molybdenum Carbide-Based Electrocatalysts for Hydrogen Evolution Reaction, Chem. - A Eur. J. 23 (2017) 10947–10961. doi:10.1002/chem.201701064.

[25] J. Zhang, T. Wang, L. Liu, K. Du, W. Liu, Z. Zhu, M. Li, Molybdenum disulfide and Au ultrasmall nanohybrids as highly active electrocatalysts for hydrogen evolution reaction, J. Mater. Chem. A. 5 (2017) 4122–4128. doi:10.1039/C6TA10385E.

[26] Y. Luo, D. Huang, M. Li, X. Xiao, W. Shi, M. Wang, J. Su, Y. Shen, MoS_2 nanosheet decorated with trace loads of Pt as highly active electrocatalyst for hydrogen evolution reaction, Electrochim. Acta. 219 (2016) 187–193. doi:10.1016/j.electacta.2016.09.151.

[27] X. Huang, Z. Zeng, S. Bao, M. Wang, X. Qi, Z. Fan, H. Zhang, Solution-phase epitaxial growth of noble metal nanostructures on dispersible single-layer molybdenum disulfide nanosheets, Nat. Commun. 4 (2013) 1444. doi:10.1038/ncomms2472.

[28] G. Kresse, D. Joubert, From ultrasoft pseudopotentials to the projector augmented-wave method, Phys. Rev. B. 59 (1999) 1758–1775. doi:10.1103/PhysRevB.59.1758.

[29] H.J. Monkhorst, J.D. Pack, Special points for Brillouin-zone integrations, Phys. Rev. B. 13 (1976) 5188–5192. doi:10.1103/PhysRevB.13.5188.

[30] S. Lu, C. Li, Y.F. Zhao, Y.Y. Gong, L.Y. Niu, X.J. Liu, Tunable redox potential of nonmetal doped monolayer MoS 2 : First principle calculations, Appl. Surf. Sci. 384 (2016) 360–367. doi:10.1016/j.apsusc.2016.05.038.

[31] D. Voiry, H. Yamaguchi, J. Li, R. Silva, D.C.B. Alves, T. Fujita, M. Chen, T. Asefa, V.B. Shenoy, G. Eda, M. Chhowalla, Enhanced catalytic activity in strained chemically exfoliated WS2 nanosheets for hydrogen evolution, Nat. Mater. 12 (2013) 850–855. doi:10.1038/nmat3700.

[32] W. Zhu, C. Tang, D. Liu, J. Wang, A.M. Asiri, X. Sun, A self-standing nanoporous MoP_2 nanosheet array: an advanced pH-universal catalytic electrode for the hydrogen evolution reaction, J. Mater. Chem. A. 4 (2016) 7169–7173. doi:10.1039/C6TA01328G.

[33] J. Deng, H. Li, J. Xiao, Y. Tu, D. Deng, H. Yang, H. Tian, J. Li, P. Ren, X. Bao, Triggering the electrocatalytic hydrogen evolution activity of the inert two-dimensional MoS_2 surface via single-atom metal doping, Energy Environ. Sci. 8 (2015) 1594–1601. doi:10.1039/C5EE00751H.

[34] J. Zhang, T. Wang, P. Liu, S. Liu, R. Dong, X. Zhuang, M. Chen, X. Feng, Engineering water dissociation sites in MoS_2 nanosheets for accelerated electrocatalytic hydrogen production, Energy Environ. Sci. 9 (2016) 2789–2793. doi:10.1039/C6EE01786J.

[35] M.N. Grisolia, J. Varignon, G. Sanchez-Santolino, A. Arora, S. Valencia, M. Varela, R. Abrudan, E. Weschke, E. Schierle, J.E. Rault, J.-P. Rueff, A. Barthélémy, J. Santamaria, M. Bibes, Hybridization-controlled charge transfer and induced magnetism at correlated oxide interfaces, Nat. Phys. 12 (2016) 484–492. doi:10.1038/nphys3627.

[36] C. Lv, C. Yan, G. Chen, Y. Ding, J. Sun, Y. Zhou, G. Yu, An Amorphous Noble-Metal-Free Electrocatalyst that Enables Nitrogen Fixation under Ambient Conditions, Angew. Chemie - Int. Ed. (2018) 1–5. doi:10.1002/anie.201801538.

[37] H. Bin Yang, S. Hung, S. Liu, K. Yuan, S. Miao, L. Zhang, X. Huang, Atomically dispersed Ni (i) as the active site for electrochemical CO 2 reduction, (2018) 1–18.

[38] L. Zhang, L. Han, H. Liu, X. Liu, J. Luo, Potential-Cycling Synthesis of Single Platinum Atoms for Efficient Hydrogen Evolution in Neutral Media, Angew. Chemie. 129 (2017) 13882–13886. doi:10.1002/ange.201706921.

[39] D. Wang, X. Zhang, Y. Shen, Z. Wu, Ni-doped MoS_2 nanoparticles as highly active hydrogen evolution electrocatalysts, RSC Adv. 6 (2016) 16656–16661. doi:10.1039/C6RA02610A.

[40] D. Escalera-López, Y. Niu, J. Yin, K. Cooke, N. V. Rees, R.E. Palmer, Enhancement of the Hydrogen Evolution Reaction from Ni-MoS_2 Hybrid Nanoclusters, ACS Catal. 6 (2016) 6008–6017. doi:10.1021/acscatal.6b01274.

[41] X. Ma, J. Li, C. An, J. Feng, Y. Chi, J. Liu, J. Zhang, Y. Sun, Ultrathin Co(Ni)-doped MoS_2 nanosheets as catalytic promoters enabling efficient solar hydrogen production, Nano Res. 9 (2016) 2284–2293. doi:10.1007/s12274-016-1115-9.

[42] B. Zhang, J. Liu, J. Wang, Y. Ruan, X. Ji, K. Xu, C. Chen, H. Wan, L. Miao, J. Jiang, Interface engineering: The $Ni(OH)_2/MoS_2$ heterostructure for highly efficient alkaline hydrogen evolution, Nano Energy. 37 (2017) 74–80. doi:10.1016/j.nanoen.2017.05.011.

[43] R. Subbaraman, D. Tripkovic, K.-C. Chang, D. Strmcnik, A.P. Paulikas, P. Hirunsit, M. Chan, J. Greeley, V. Stamenkovic, N.M. Markovic, Trends in activity for the water electrolyser reactions on 3d M(Ni,Co,Fe,Mn) hydr(oxy)oxide catalysts, Nat. Mater. 11 (2012) 550–557. doi:10.1038/nmat3313.

[44] L.-L. Feng, G. Yu, Y. Wu, G.-D. Li, H. Li, Y. Sun, T. Asefa, W. Chen, X. Zou, High-Index Faceted Ni_3S_2 Nanosheet Arrays as Highly Active and Ultrastable Electrocatalysts for Water Splitting, J. Am. Chem. Soc. 137 (2015) 14023–14026. doi:10.1021/jacs.5b08186.

[45] C. Tsai, F. Abild-Pedersen, J.K. Nørskov, Tuning the MoS 2 Edge-Site Activity for Hydrogen Evolution via Support Interactions, Nano Lett. 14 (2014) 1381–1387. doi:10.1021/nl404444k.

[46] H.I. Karunadasa, E. Montalvo, Y. Sun, M. Majda, J.R. Long, C.J. Chang, A Molecular MoS2 Edge Site Mimic for Catalytic Hydrogen Generation, Science (80-.). 335 (2012) 698–702. doi:10.1126/science.1215868.